HHS Public Access

Author manuscript

Aerosol Sci Technol. Author manuscript; available in PMC 2026 January 15.

Published in final edited form as:

Aerosol Sci Technol. 2025 ; 59(10): 1198–1209. doi:10.1080/02786826.2024.2442524.

Cellular responses of lung cells cultured at an Air-liquid Interface are influenced by spatial nanoparticle deposition patterns in an *in vitro* aerosol exposure system

Sripriya Nannu Shankar[1,2,*], **Amber O'Connor**[3,*], **Kiran Mital**[4], **Yuetong Zhang**[1,5], **Alex Theodore**[1], **Amin Shirkhani**[1,6], **Stavros Amanatidis**[7], **Gregory S. Lewis**[7], **Arantzazu-Eiguren Fernandez**[7], **Trevor B. Tilly**[8], **Otmar Schmid**[9], **Tara Sabo-Attwood**[3], **Chang-Yu Wu**[1,6]

[1]Department of Environmental Engineering Sciences, University of Florida, Gainesville, Florida, USA

[2]Department of Environmental & Public Health Sciences, University of Cincinnati, Cincinnati, Ohio, USA

[3]Department of Environmental & Global Health, University of Florida, Gainesville, Florida, USA

[4]Department of Mechanical Engineering, University of Florida, Gainesville, Florida, USA

[5]Department of Mechanical Engineering, University of British Columbia, Vancouver, British Columbia, Canada

[6]Department of Chemical, Environmental & Materials Engineering, University of Miami, Miami, Florida, USA

[7]Aerosol Dynamics Inc., Berkeley, California, USA

[8]711[th] Human Performance Wing, Air Force Research Laboratory, Wright-Patterson Airforce Base, Ohio, USA

[9]Insitute of Lung Health and Immunity, Helmholtz Munich, Neuherberg/Munich, Germany

Abstract

The deposition of inhaled particles is typically highly localized in both the bronchial and alveolar region of the lung displaying spot-like, line-like and other deposition patterns. However, knowledge is very limited on how different deposition patterns may influence downstream cellular responses. In this study, the Dosimetric Aerosol *in Vitro* Inhalation Device (DAVID) was used for dose-controlled deposition of cupric oxide nanoparticles (CuONPs) in four different patterns (i.e., spot, ring, line and circle) on human alveolar A549 cells cultured at an air-liquid interface (ALI). After CuONP deposition (<15 min) and a 24 h incubation phase, cell viability, apoptotic / necrotic cell count, and gene expressions were measured. At the lowest dose of ~5 μg/cm^2, the line pattern resulted in the lowest viability of cells (57%), followed by the spot pattern (85%) while the ring and circle patterns exhibited >90% viability, compared to the particle free air control. At the highest dose of ~20 μg/cm^2, the viability reduced to 44%-60% for all patterns.

CONTACT Sripriya Nannu Shankar nannussa@ucmail.uc.edu Division of Environmental & Industrial Hygiene, Department of Environmental & Public Health Sciences, College of Medicine, University of Cincinnati, OH 45267, USA.
*To be considered joint first authors

Also, the gene profile was found to depend on deposition pattern. The results demonstrate that the deposition pattern is a critical parameter influencing cellular response, thus an important parameter to consider in toxicity and drug delivery studies. Furthermore, the ability of DAVID to control the delivery of aerosolized particles in various deposition patterns was demonstrated, which enables implementation of nonhomogeneous particle deposition patterns that mimic real-life human inhalation exposures in future *in vitro* toxicology studies.

Graphical Abstract

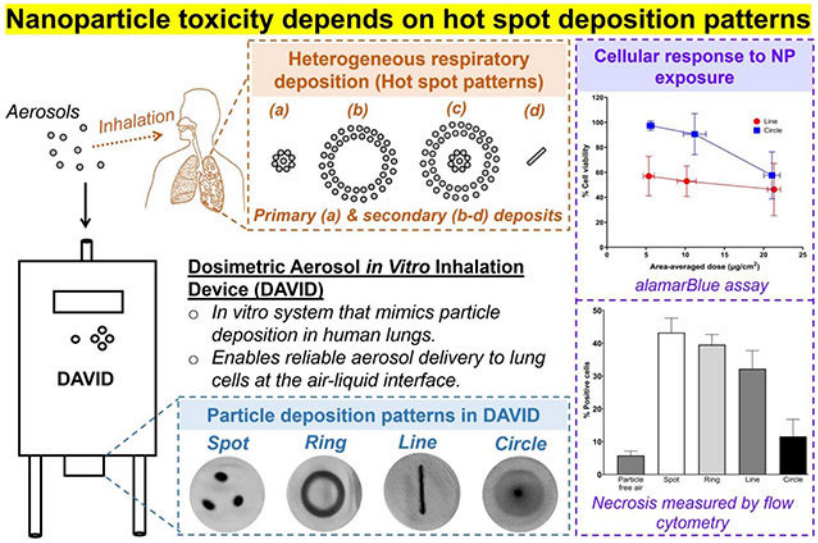

Keywords

Aerosol delivery; *in vitro* inhalation toxicology; respiratory deposition; global dose; hot spot dose; new approach methods (NAMs)

1. Introduction

The deposition of inhaled particulates within various regions of the respiratory tract can influence the body's biological response to these insults. Several variables (such as particle size and shape, mass, flow rate, age, gender, underlying health conditions, etc.,) affect how and where inhaled particles deposit within the airways (Hussian et al., 2011). Regional deposition of inhaled aerosol particles depends on respiratory parameters (tidal volume and respiratory frequency) as well as particle size (hygroscopicity), density and shape. For spontaneous nose breathing, larger particles (>2.5 μm) deposit in the upper airways whereas smaller particles (< 2.5 μm) can reach the distal and even alveolar regions of the lung (Carvalho et al., 2011; Li et al., 2018). Site specific deposition of particulates in these regions has been associated with primary locations of cancer development (Schlesinger et al., 1978) suggesting that the occurrence of adverse health outcomes can be greatly influenced by particle deposition within specific regions of the respiratory tree (Franck et al., 2011; Li et al., 2018).

Particle deposition in the respiratory system was first demonstrated in experimental studies in the 1970s using hollow casts of the human tracheobronchial tree (Schlesinger et al., 1978), although much of our particle deposition knowledge is garnered from computational simulations and image analysis. Some of these models address the idea that particles are not only deposited in different regions of the lung (i.e. tracheobronchial, terminal bronchioles, alveolar duct, etc.,), but they are also non-uniformly deposited in each region. For instance, Balásházy et al. (2003) showed a high degree of heterogeneity regarding particle deposition along the bronchial airway surface via computational fluid dynamics modeling. Hoffmann et al. (2001) showed that, in the upper airways where bifurcations of bronchi occur, particles are deposited by inertial forces and convective diffusion, which have been observed in animal models as defined circular or elliptical spots (Porra et al., 2018). Repeated bifurcations cause the flow to be in a continual state of development, resulting in secondary flow formation and turbulence (Kaye and Phillips 1997), thereby producing varying non-uniform deposition patterns. Moreover, there is empirical and computational evidence that micron-sized aerosols display a line-like “hot spot” deposition pattern in the proximal alveolar range due to gravitational settling along the centerline of the alveolar duct (Anjilvel and Asgharian 1995; Yang et al., 2019; Gradl et al., 2019). In contrast, toxicological *in vitro* cell culture experiments are almost exclusively performed with relatively uniform aerosol deposition patterns (Paur et al., 2011). In general, impacting particles can deposit in different patterns such as rings, halos, circular drops, lines, and disks due to bounce effects (Soysal et al., 2021), depending on factors such as particle characteristics, lung geometry, age, gender, etc., albeit it is not clear to what extent this also occurs on liquid-coated surfaces such as the lung epithelium. Particles deposited in localized, highly concentrated patterns can result in local tissue doses that are several hundred times higher than the average dose of the whole airway/lung structure (Balásházy et al., 2003). Therefore, it is worth considering the impact that inhomogeneous particle deposition patterns may have on cellular responses, as this can influence aerosol drug efficacy and particle toxicity studies.

Understanding the specific cellular and molecular changes in response to different deposition patterns of aerosolized particles *in vitro* is challenging. Several commercial aerosol exposure devices exist (such as Vitrocell®, XposeALI®, and CULTEX®), but most do not have the capability to generate varied particle deposition patterns. Thus, establishing a system that better resembles the *in vivo* situation by facilitating different deposition patterns is desirable. This approach is also in line with the United States Environmental Protection Agency’s 3R principle which supports replacement, reduction, and refinement of animal testing with advanced *in vitro* approaches (USEPA, 2023). The Dosimetric Aerosol *in Vitro* Inhalation Device (DAVID) has been demonstrated to efficiently deliver particles as spot to cells (Tilly et al., 2019; Tilly et al., 2023). Here we expand DAVID’s capability to facilitate delivery of airborne particles with different particle deposition patterns (i.e. spot, line, ring, and circle) to lung cells cultured at the air-liquid interface (ALI). Using this exposure system, we investigated the effect of deposition patterns of aerosolized cupric oxide nanoparticles (CuONPs) on cellular responses.

2. Methodology

2.1. Exposure system for delivery of airborne particles

Designed by Aerosol Dynamics Inc., USA, DAVID collects airborne particles through laminar flow and water-based condensational growth, delivering amplified particles to cells cultured at the ALI. The system was initially designed to deliver particles onto commercial Petri dishes and later modified to accommodate cell exposures. Its working principle and operating conditions have been described previously (Tilly et al., 2019; Ward et al., 2020; Tilly et al., 2023; Nannu Shankar et al., 2023). Briefly, DAVID consists of 8 growth tubes in 3 sections, through which incoming particles travel. The sections are set at different temperatures – a conditioner at 4 °C to cool the incoming particles, an initiator at 40 °C to provide supersaturation for particle growth and a moderator at 25 °C to remove excess moisture. The amplified particles are deposited on a 35 mm × 10 mm Petri dish set at 37 °C through a nozzle plate at 30 °C. At the set temperatures, the relative humidity of the flow exiting DAVID was >95%, while that at the inlet of DAVID, i.e., after dilution of aerosols was <5%. For the current study, the collection unit comprising the nozzle plate and the sample holder was custom designed to facilitate delivery of airborne particles in multiple patterns to cells cultured at the ALI. Two nozzle plates corresponding to 4 growth tubes, with either 3 round nozzles (Figure 1a) or 1 rectangular nozzle (Figure 1d) for each growth tube were designed, such that their areas remained similar (2 mm^2 for rectangular nozzles and 2.6 mm^2 for round nozzles). Particle delivery through these nozzles resulted in 3 spots (Figure 1b) or line (Figure 1e) patterns, corresponding to the nozzle design.

The sample holder was designed to accommodate cell culture Transwell® inserts (Polyester membrane of area 0.33 cm^2, 0.4 μm pore size, Corning, USA) or polystyrene (PS) transparent wells of similar surface area (Fisher Scientific, USA)). The PS wells were used for dosimetry, while the Transwell® inserts were used for cell exposures. A worm gear motor connected to the 4 wells of the sample holder through individual shafts enabled rotation on their axes (Figure 2b). When the motor was turned on, particles were deposited as a ring (Figure 1c) and circle (Figure 1f), for the round and rectangular nozzles, respectively.

2.2. Experimental setup

The setup comprised of aerosol generation, dilution and collection as presented in Figure 2a. Cupric oxide (CuO) powder (25-55 nm, specific surface area 13.98 m^2/g; equivalent geometric mass-specific surface area: 17 m^2/g (diameter: 40 nm; 8.96 g/cm^2), >99.95% purity, US Research Nanomaterials Inc., USA) suspended in 190 proof ethanol at varying concentrations (0.1, 0.5 and 1 mg/mL) was sonicated for 30 min at 50-60 Hz. These nebulizer concentrations were selected based on the working concentrations determined in our previous study (Nannu Shankar et al., 2023). Aerosols generated from these suspensions using a 6-jet Collison nebulizer (CH Technologies, USA) operated at 5 LPM were diluted with 15 LPM of compressed air (breathing grade, AirGas, USA), and then fed into the DAVID operated at a sample flow rate of 2 LPM. The particle size distribution was monitored by a Scanning Mobility Particle Sizer (SMPS) that consisted of an electrostatic classifier (Model 3080, TSI Inc., USA), differential mobility analyzer (Model 3081, TSI

Inc., USA) and condensation particle counter (Model 3022A, TSI Inc., USA) to monitor the CuONP aerosol size distributions (Figure S1). Through a high-efficiency particulate arresting (HEPA) filter, excess flow in the experimental setup was discharged.

2.3. Determination of doses delivered through DAVID

The particles delivered to 4 PS wells in DAVID after 15 min of aerosolization were subjected to acid digestion as previously described (Nannu Shankar et al., 2023), which were then analyzed by inductively coupled plasma-optical emission spectrometry (ICP-OES, Spectro Arcos I or II). The area-averaged doses were quantified as:

$$Dose = \frac{Mass\ of\ CuO\ deposited}{Area\ of\ the\ insert\ or\ PS\ well} = \frac{C \times V_s \times M_{CuO}}{M_{Cu} \times A_{well}} \quad (1)$$

where C is the mass concentration of Cu from ICP-OES analysis (μg/mL), V_s is the volume of acid-digested sample (10 mL), M_{CuO} is the molar mass of CuO (79.55 g/mol), M_{Cu} is the molar mass of Cu (63.55 g/mol), and A_{well} is the deposition area of the insert or PS well (0.33 cm^2). Localized doses (henceforth abbreviated as hot spot doses) were calculated according to Eq. 1 but using the area calculated by ImageJ analysis corresponding to each deposition pattern (0.03, 0.09, 0.02 and 0.23 cm^2 for spot, ring, line and circle, respectively). The doses are expressed as μg/cm^2. For cell exposures, the Cu concentration in the nebulizer and the duration of aerosol-cell exposure were varied between 0.1 and 1 mg/mL and 5 and 15 min, respectively, to achieve same target doses (~5, 10 and 20 μg/cm^2) for all the deposition patterns (Table S1). Dose focusing factors were calculated from the ratio of hot spot doses and area-averaged doses. A comparison of the dose focusing factors was made based on the hot-spot doses determined from the (1) areas per the nozzle geometry (termed as ‘theoretical dose focusing factors’) and (2) areas estimated by ImageJ analysis (termed as ‘actual dose focusing factors’).

2.4. Cell culture

For all cell studies, a human lung adenocarcinoma cell line representing an alveolar epithelial type II like cell was employed (A549; CCL-185, American Type Cell Collection (ATCC), Manassas, VA, USA) to generate ALI cultures based on a previous protocol (Tilly et al., 2023) with some modifications. Briefly, cells were seeded on 6.5 mm diameter Transwell® inserts (0.33 cm^2; polyester, 0.4 μm pore size; CellTreat Scientific Products, Cat# 50-153-5162) in each well of a 24-well plate (CellTreat Scientific Products, MA, USA). Prior to seeding, each insert was coated with 100 μL of 30 μg/mL rat tail collagen coating solution (Cell Applications, Inc., Cat# 122-20, San Diego, CA) diluted in phosphate buffered saline (PBS) (Cytiva HyClone, Cat# SH3025601, Logan, UT). After a 45-min incubation, the collagen solution was aspirated and then each insert was washed with PBS. A549 cells were seeded at ~50,000 cells/insert in 100 μL Roswell Park Memorial Institute (RPMI) 1640 medium supplemented with 1% Glutamax (Gibco, Cat# 35050-06, Grand Island, NY), 10% heat-inactivated fetal bovine serum (FBS) (HyClone, Logan, UT), and 1% Penicillin-Streptomycin-Neomycin (PSN) (Gibco, Cat# 15-040-CV, Grand Island, NY). An additional 500 μL of RPMI medium was added to the basal chambers of all wells. The

cells were maintained in an incubator at 37 °C and 5% CO_2. Upon confluency (~24 h after seeding), the apical medium was removed and fresh RPMI medium (500 μL) was added to the basal chambers every 48 hrs. After 7 days of culture at the ALI, cells were exposed to CuONPs at 5.4±0.1, 10.8±0.4 and 20.8±0.5 μg/cm^2. For all cell exposures, 3 Transwell® inserts (containing A549 cells) and 1 PS well (for dosimetry) were used concurrently. Clean-air exposed cells were used as sham control and unexposed A549 cells in the incubator served as negative (incubator) controls. Since there was no significant difference in viability or gene expression observed between the particle free air controls and incubator controls (Figure S2), exposure to the DAVID system itself did not induce any biological response; all the treatment groups were compared to the respective particle free air (sham) controls. Cells were evaluated for viability, gene expression, and necrosis and apoptosis 24 h post exposure.

2.5. Cell viability by alamarBlue assay

The alamarBlue® assay (Bio-Rad, Cat# BUF012A, Hercules, CA) was performed according to the protocol described by the manufacturer, to assess cellular mitochondrial activity as a measure of viability. The apical cell surface was washed with PBS and the cells were incubated with 200 μL of 10% alamarBlue solution for 1 h at 37 °C. Then, 100 μL of the 10% alamarBlue solution was withdrawn and added into a black clear bottom 96-well plate (Corning, USA). Fluorescence was quantified at 570 nm (excitation) and 590 nm (emission) using a microplate reader (Synergy H1, Biotek, Winooski, VT). The % cell viability was calculated from the ratio of the emission fluorescence of the experimental groups (i.e., cells exposed to CuONPs) and the particle-free air control group (i.e., cells exposed to particle-free air by connecting a HEPA filter at DAVID's inlet).

2.6. RNA isolation and gene expression

Cell lysates were collected from each insert in 750 μL RNA STAT-60 Reagent (Tel-Test, Inc. Friendswood, TX) and vortexed to promote lysis. RNA/mRNA extraction and purification was performed as previously described by Smith et al. (2018). RNA was quantified using a Synergy™ H1 plate reader (BioTek Instrument, Inc., Winooski, VT) and DNase-treated using the RapidOut DNA Removal Kit (ThermoFisher, Ref# K2981, Vilnius, Lithuania), and then reverse transcribed using the High-Capacity cDNA Reverse Transcriptase Kit (ThermoFisher, Ref# 4368813, Vilnius, Lithuania). cDNA was diluted 1:10 in RNase-DNase free H_2O and amplified using validated primers for heme oxygenase-1 (HMOX1) and interleukin-8 (IL-8), per Chen et al. (2019). Target gene expression was normalized to glyceraldehyde 3-phosphate dehydrogenase (GAPDH) and quantified using the ΔΔCt method (Chen et al., 2019; Smith et al., 2018).

2.7. Cell necrosis and apoptosis

Following exposure to ~10 μg/cm^2 of CuONPs, A549 cells were dissociated from the insert with TrypLE™ Express trypsin (Gibco, Cat# 12604013, Grand Island, NY) followed by gentle up-and-down pipetting. The cells were washed with cold PBS and centrifuged at 350 relative centrifugal force (rcf) at 4 °C for 5 min. Cells were stained with a fluorescein isothiocyanate (FITC)-conjugated Annexin V (AV) and propidium iodide (PI) kit (ThermoFisher Scientific, Inc., Cat# V13242, Eugene, OR). Cells (~10^5) were then resuspended in 100 μL AV binding buffer and stained with 0.5 μL Alexa Fluor 488 conjugate

for 15 min. PI was added immediately before analysis at a final concentration of 1.5 μg/mL. AV binding buffer (400 μL) was then added to each sample and the cells were analyzed on the Cytoflex LX cytometer. Data analysis was conducted using Flowjo v10.2 software and gated on doublet-excluded cells. An example of the gating strategy for cells exposed to particle-free air is presented in Figure S3.

2.8. Statistical analysis

The cell exposure and dosimetry results are presented as mean ± standard deviation of three and four technical replicates, respectively, across three independent experiments. All statistical analyses were performed in GraphPad Prism (Version 10.0.0). A one-way ANOVA Tukey's multiple comparisons was used to test the variations between doses for a given pattern or the variations between patterns for a given dose. Statistical differences between groups are indicated on the graphs by an asterisk (✱) for $p \leq 0.05$.

3. Results

3.1. Dosimetry in DAVID

ImageJ analysis revealed that the circle pattern covered 68% of the total area of the insert or well, followed by the ring (27%), spot (10%) and line (7%). A nebulizer suspension of 0.1 mg/mL produced a CuONPs dose (area-averaged) of 27.2±1.5 μg/cm^2 when delivered as spot, 26.5±1.6 μg/cm^2 as ring, 5.7±1.1 μg/cm^2 as line and 6.1±0.6 μg/cm^2 as circle. With increasing nebulizer concentrations, higher doses were delivered (Figure 3). For nebulizer concentrations of 0.5 and 1 mg/mL, doses of the following ranges were obtained: 50.5±3.2 and 137.2±19.8 μg/cm^2 for spot; 45.3±3.5 and 140±13.6 μg/cm^2 for ring; 26.3±2.2 and 60±12.8 μg/cm^2 for line and 28.7±3.3 and 59.1±6.6 μg/cm^2 for the circle. All the above-mentioned doses were achieved in 15 min.

As can be inferred from Figure 3a, there was no significant difference between the doses delivered by different patterns of the same nozzle design (i.e., spot and ring; or line and circle). However, there was a significant difference ($p \leq 0.0001$) in doses delivered by the 2 nozzle designs (i.e., round vs. rectangular) which could be attributed to differences in their geometry and corresponding cutoff diameters (Dp_{50} i.e., the particle size at which 50% of particles are collected). The theoretical Dp_{50} (calculated according to equations in section S1) were 2 and 2.36 μm for round and rectangular nozzles, respectively. At the lowest nebulizer concentration (i.e., 0.1 mg/mL), the doses delivered by the round nozzles were about 4-5 times higher than those delivered by the rectangular nozzles. The ratio of the doses delivered by the round vs. rectangular nozzles was ~1.6-2.4 for 0.5 mg/mL and 1 mg/mL. Figure 3b illustrates the hot spot doses for different patterns, which vary by a dose focusing factor (Figure S4). As can be seen from Figure S4, the hot spot dose focusing factor was higher for patterns with lower deposition area.

3.2. Cellular response post exposure to CuONPs

3.2.1. Cell viability: Cell viability decreased in a dose-dependent manner following CuONPs exposure in circle, ring, or spot patterns (Figure 4). At the lowest dose of ~5 μg/cm^2, the line pattern resulted in the greatest impact on cell viability (57%), followed

by the spot pattern (85%) while the ring and circle patterns exhibited >90% cell viability. Of note, only the line pattern resulted in a decrease in cell viability that was significantly reduced compared to control ($p < 0.05$). At ~10 μg/cm^2, viability recorded for the circle (91%) was not significantly different from control, whereas the other patterns showed a range in viability (53-79%) with the line pattern having the lowest viability. At the highest dose of ~20 μg/cm^2, viability was significantly reduced to 44%-60% with the greatest effects occurring for the ring pattern. Furthermore, there was no significant difference in viability between patterns at ~20 μg/cm^2.

Analysis by flow cytometry post cell exposures showed that there was a significant increase in the percentage of apoptotic cells for the line and circle patterns at a dose of ~10 μg/cm^2, compared to particle free air (sham). However, there was no significant difference in the percentage of apoptotic cells among the line, spot, and circle patterns (Figure 5). Additionally, there was a significant increase in the percentage of necrotic cells for the line, ring, and spot patterns compared to particle free air (sham).

3.2.2. Gene expression: Following a 24 h treatment of A549 cells with CuONPs (doses 5.4±0.12 and 10.76±0.42 μg/cm^2), 10- to 20-fold upregulated expression ($p < 0.05$) of HMOX1 relative to clean air (sham) exposure was recorded for all deposition patterns (Figure 6). There was no dependance of HMOX1 on deposition pattern for the low dose (5 μg/cm^2), but for the 10 μg/cm^2 there was a ca. 2-fold reduced HMOX1 expression for the line pattern as compared to the spot and ring patterns (Figure 6). Also, the circle pattern showed lower HMOX1 expression than the spot and ring pattern, but on a non-significant level. Analogous trends were observed for IL-8 induction, yet largely on a non-significant level due to the lower IL-8 induction levels (2 –4-fold, Figure 7) as compared to those of HMOX1 (Figure 6).

4. Discussion

Historically, particle toxicology studies with cell models were performed for uniform particle-cell deposition patterns. Great care was taken that uniform aerosol-cell deposition patterns were established by using well-mixed aerosol and/or radially symmetric (stagnation point) flow conditions (e.g. Bitterle et al. 2006, Lenz et al., 2009) matching the circular cell growth area on Transwell® inserts. Uniform aerosol deposition simplifies determination of the cell-deposited particle dose per exposed cell area, which is the most relevant dose metric for extrapolation of *in vitro* to *in vivo* particle toxicology (Schmid and Cassee 2017). However, uniform aerosol deposition is rarely found in human (or animal) lungs. Mainly spot- and line-like deposition patterns are formed on or near the carinal ridge of bifurcations in the bronchial region and along the centerline of the alveolar ducts due to inertial impaction and gravitational settling for larger particles (aerodynamic diameter larger than 500 nm) and due to secondary flow formation for 10 to 500 nm aerosol (Balásházy et al., 2003; Hofmann 2011; Anjilvel and Asgharian 1995; Yang et al., 2019; Gradl et al., 2019). While dose focusing factors (relative to uniform deposition) near airway bifurcations have been determined from computational models to reach up to 400 depending on aerosol size and respiratory conditions, focusing factors for the alveolar region are not that well known, yet. The toxicological relevance of these hot spot deposition patterns is not well

understood, yet the frequent initial occurrence of bronchial lung cancer lesions near airway bifurcations has been interpreted as a result of hot spot deposition of toxic particles (e.g. cigarette smoke, urban aerosol) in this region (Balásházy et al., 2003). Further investigation of the effect of localized particle deposition on particle-induced lung toxicity would benefit from aerosol-cell deposition technologies facilitating hot spot aerosol deposition.

Using a specially designed collection unit for DAVID, we were able to validate the performance of the system in delivering consistent doses of aerosolized CuONPs in 4 patterns to the apical surface of lung cells cultured at ALI. Based on the data presented in Figure S5, the coefficient of variation (CV, i.e., ratio of standard deviation to the mean) for dosimetry across triplicate experiments and across the four well positions were <20% depending on the nebulizer concentrations and is comparable to commercially available exposure systems. For example, the variations within the Vitrocell® AMES 48 system was reported as 15-45% depending on particle dose (Oldham et al. 2020a, 2020b), and a novel prototype flatbed exposure system termed NAVETTA reported <5% to ~17% of the total Cu across all of the Transwell® inserts that was contingent on their position (Frijns et al., 2017). In the air-liquid interface cell exposure system (ALICE), spatially uniform dose was achieved with insert-to-insert variability <1.6% and an insert-averaged dose repeatability of <12% for different types of materials (Lenz et al., 2009). For the Vitrocell® Cloud 6, the insert-to-insert dose variability was measured as 4.3% (Lenz et al., 2014). As demonstrated in our previous study with DAVID, CV of <10% can be achieved by further varying the experimental conditions (Nannu Shankar et al., 2023), which is at the lower end of the reported range of CV. For dose-targeted cell exposures, experimental parameters were varied to achieve ~5, 10 and 20 μg/cm^2 across different deposition patterns, and the doses had a CV in the range of 4-15% (Table S1).

The doses used for cell exposures fall within the lifetime exposure limit of 5.88 – 58.82 μg/cm^2 calculated based on the workplace exposure limit for Cu dust and fume set by the Occupational Safety and Health Administration (OSHA), the National Institute for Occupational Safety and Health (NIOSH), and the American Conference of Governmental Industrial Hygienists (ACGIH) (NJHealth 2016) as explained in section S2 of the online supplemental information.

If particle deposition pattern is expected to influence the cell response, the outcome measures (i.e., gene expression and viability) should depend on deposition patterns for the same dose. This study reports some notable differences in cell viability and gene expression depending on particle deposition pattern, suggesting the importance of considering this variable when conducting toxicity studies. The most significant effects were seen for the line deposition pattern of CuONPs, which significantly decreased cell viability especially for the low dose range (5–10 μg/cm^2) and mitigated the induction of HMOX1 expression. Albeit these trends appear contradictory, it is important to note that mRNA regulation is time-dependent and reaches its maximum level within a few hours after particle deposition. Thus, a single mRNA measurement at a relatively late time point (here: 24 h) may not adequately reflect the relative toxicity of the different pattern. On the other hand, cell viability occurs later and is therefore a more representative measure of toxicity suggesting that the line pattern displays the highest toxicity level of all deposition patterns tested here.

This result is consistent with the highest hot spot dose focusing factor of 13.65 (Figure S4), which is due to the smallest fractional insert area covered by the line deposition pattern (7% of the insert) as compared to the circle pattern which covered a larger surface area (68% of the insert). Interestingly, despite the line and spot patterns covering a similar surface area (7 and 10% respectively), the cell viability of the spot pattern was not different from the other two deposition patterns. This indicates that not only the hot spot dose focusing factor, but also the "shape" of the deposition pattern has an impact on dose-specific toxicity with the line pattern being most toxic – at least on Transwell® inserts. At the highest dose of ~20 μg/cm^2, there was no significant difference in viability between any patterns, which demonstrates that differences noted between deposition patterns are most pronounced for the low dose (i.e. low effect) level. Notably, exposure to the sham control and the DAVID system itself did not induce any biological response.

Taken together, our *in vitro* data support the hypothesis that non-uniform and especially line-like particle deposition enhances the toxicological response of lung cells to deposited particles. This aligns with a possible explanation that hot spot deposition patterns as seen in the lung may induce higher toxicological responses than uniformly distributed NPs as typically used for *in vitro* studies (Monteiller et al., 2007). Thus, technologies with high accessibility, consistency and reproducibility for non-uniform aerosol-cell deposition and onto commercially available Transwell® inserts, as presented in this study, are highly relevant for future particle toxicity studies. To the best of our knowledge, DAVID is the first *in vitro* exposure system to address the challenges of non-uniform NP deposition in inhalation toxicology (such as mimicking human respiratory system, representing particles in different deposition patterns and facilitating exposures to cells cultured at the ALI) in a single unit.

We acknowledge that this study has certain limitations and challenges. Firstly, even though the deposition in the circle pattern was assumed to be uniform, it was evident that there was a gradient with a more concentrated deposit at the center (the area of the center deposit was about 8% of the circle deposition pattern and 6% of the total insert's area). It was challenging to quantify the dose at the center and the periphery separately due to the nature of the gradient. The appearance of a more concentrated spot in the center of the circle pattern occurs due to the rectangle nozzle design and laminar flow through DAVID, resulting in the air flow focused on the center. Differences in delivered doses between the round and rectangular nozzle designs, for the same nebulizer concentrations and exposure times, are attributed to different geometries of the nozzle designs. It was challenging to predict the flow path using computational fluid dynamic models because the geometries were more complex than typical impactors. Nevertheless, similar delivered doses were achieved by modifying the experimental parameters such as nebulizer concentration and time. To achieve more spatially uniform deposition, other nozzle designs such as multiple nozzle orifices, a pie, or nozzles with diameters different from that used in this study are recommended in future studies. Alternately, modifying the collector unit to rotate in parabolic curves or other geometric patterns may improve homogeneity of deposition. Modifying the nozzles to produce different patterns while delivering particles over similar surface areas can facilitate better comparison of cellular responses, but careful considerations (such as the particle

trajectory through the nozzle, cut-off diameter, impaction velocity, jet velocity, etc.) should be made during design to meet high deposition efficiencies.

Secondly, particle deposition beyond defined margins was noticed when the deposition pattern was observed under a microscope after cell exposures (Figure S6), which contributed to lower dose focusing factors compared to the theoretical values (Figure S4). Deposition can depend on the impaction surface characteristics, particle type, particle loading on the impaction surface and sampling conditions (such as temperature, relative humidity, time, DAVID parameters, etc.) (Lai et al., 2008; Kala and Saylor 2021). Moisture from condensational particle growth, liquid on the cells and/or cell-to-cell transmission of particles after deposition might have also contributed to the inhomogeneity of the deposition patterns. Though our approach was not able to delineate whether particles were deposited in several layers, using advanced microscopy and imaging methods in future studies may provide a more accurate measure of the actual surface area occupied by deposited particles and potentially the dose internalized in the cells.

Thirdly, our study was designed to compare the effect of different non-uniform NP deposition patterns on the global cellular response to establish the relevance of NP deposition patterns for NP toxicity studies. Therefore, we lacked assays to distinguish the response of cells that were directly exposed to CuONPs from cells onto which CuONPs were not deposited. In such exposure scenarios, hot spot deposition of particles is a key determinant of clinical efficacy (Balásházy et al., 2003; Porra et al., 2018; Corley et al., 2021). When information on the deposition area or associated parameters to estimate the hot spot dose is unavailable, a global lung parameter (such as global lung volume or epithelial lung surface area) is a necessary simplification to obtain global (area-averaged) dose (Greenblatt et al., 2015). As can be seen in Figure S7, the ability to deliver particles in distinct patterns through DAVID enables a comparison of cellular response with respect to both – area-averaged and highly localized doses. Such a comparison reveals sharper slopes for the deposition patterns covering greater surface areas (i.e., ring and circle) in comparison to focused patterns (spot and line), which suggests cellular interactions vary for different particle deposition patterns. However, correlation of cellular responses with hot spot doses was not possible with the assays used here. Moreover, only the expressions of 2 genes (HMOX1 and IL8) were measured in this study and only at a single rather “late” time point (24 h after exposure). Robust analysis methods for gene profiling (such as microarrays, RNA-seq, etc.,) possibly at an earlier time point (e.g. 6 h) can yield better insights on the correlation between doses, deposition patterns and different biomarkers. Future studies focusing on toxicity analysis from a mechanistic standpoint with an emphasis on hot spot doses are warranted.

Finally, this study used a human lung adenocarcinoma cell line, i.e., A549 cells, to validate the performance of DAVID in delivering aerosols in different patterns. Development and exposure assessment of robust cell models, such as differentiated cells with beating cilia, co-cultures, 3D constructs, organoids, etc., that better mimic human lung are warranted. Nevertheless, our study is among the first to provide proof-of-concept on the significance of deposition patterns and consideration of hot spot doses in inhalation toxicology.

5. Conclusions

Deposition of inhaled particles in the respiratory tract occurs in differently shaped and pronounced hot spot patterns depending on particle characteristics and the respiratory mechanics of an individual. Our *in vitro* study with CuONPs and lung cells is among the first to provide proof-of-concept on the significance of deposition patterns and consideration of hot spot doses in inhalation toxicology. In this study, aerosolized CuONPs were deposited onto ALI-cultured human A549 lung cells in four different patterns (spot, ring, line, and circle) harnessing a refined version of the DAVID system. We observed dose-dependent differences in cell viability and gene expression dependent on particle deposition pattern. At lower doses (~5 and 10 μg/cm^2) associated with lower effect levels, cell viability was significantly reduced relative to sham control for the line shape pattern only. There was no significant difference in viability across deposition patterns at the highest dose (~20 μg/cm^2) of CuONPs. HMOX1 mRNA was downregulated for the line pattern and to a lesser degree for the circle pattern (strong trend – not significant). These results provide evidence that not only dose but (hot spot) deposition patterns are critical parameters in toxicological cellular responses *in vitro.* In addition, the study highlights the applicability of DAVID in controlled delivery of particles in different patterns to cells at the ALI. Future studies assessing the relative importance of hot spot versus uniform particle deposition on localized and global cellular responses with consideration of dosimetry are necessary to advance *in vitro* inhalation toxicology.

Supplementary Material

Refer to Web version on PubMed Central for supplementary material.

Acknowledgments

The authors thank UF-IFAS analytical services lab for ICP-OES analysis.

Funding

This study was funded by NIH Grant No. R44ES030649 and partly supported by the National Center for Advancing Translational Sciences of the NIH under UF and FSU CTS Awards TL1TR001428 & UL1TR001427. Tuition for SN was partially paid by UF-HWCoE.

References

Anjilvel S, & Asgharian B (1995). A multiple-path model of particle deposition in the rat lung. Fundamental and Applied Toxicology 28(1), 41–50. doi: 10.1006/faat.1995.1144. [PubMed: 8566482]

Balásházy I, Hofmann W, & Heistracher T (2003). Local particle deposition patterns may play a key role in the development of lung cancer. J Appl Physiol 94(5):1719–1725. doi:10.1152/japplphysiol.00527.2002. [PubMed: 12533493]

Bitterle E, Karg E, Schroeppel A, Kreyling WG, Tippe A, Ferron GA, … & Hofer T (2006). Dose-controlled exposure of A549 epithelial cells at the air–liquid interface to airborne ultrafine carbonaceous particles. Chemosphere 65(10), 1784–1790. doi:10.1016/j.chemosphere.2006.04.035. [PubMed: 16762398]

Carvalho TC, Peters JI, & Williams RO III (2011). Influence of particle size on regional lung deposition–what evidence is there? International journal of pharmaceutics 406(1-2):1–10. doi:10.1016/j.ijpharm.2010.12.040. [PubMed: 21232585]

Chen H, Humes ST, Robinson SE, Loeb JC, Sabaraya IV, Saleh NB, … & Sabo-Attwood T (2019). Single-walled carbon nanotubes repress viral-induced defense pathways through oxidative stress. Nanotoxicology 13(9):1176–1196. doi:10.1080/17435390.2019.1645903. [PubMed: 31328592]

Corley RA, Kuprat AP, Suffield SR, Kabilan S, Hinderliter PM, Yugulis K, & Ramanarayanan TS (2021). New approach methodology for assessing inhalation risks of a contact respiratory cytotoxicant: Computational fluid dynamics-based aerosol dosimetry modeling for cross-species and *in vitro* comparisons. Toxicological Sciences 182(2), 243–259. doi:10.1093/toxsci/kfab062. [PubMed: 34077545]

Franck U, Odeh S, Wiedensohler A, Wehner B, & Herbarth O (2011). The effect of particle size on cardiovascular disorders—The smaller the worse. Science of the Total Environment 409(20):4217–4221. doi:10.1016/j.scitotenv.2011.05.049. [PubMed: 21835436]

Frijns E, Verstraelen S, Stoehr LC, Van Laer J, Jacobs A, Peters J, … & Himly M (2017). A novel exposure system termed NAVETTA for *in vitro* laminar flow electrodeposition of nanoaerosol and evaluation of immune effects in human lung reporter cells. Environmental Science & Technology 51(9):5259–5269. doi:10.1021/acs.est.7b00493. [PubMed: 28339192]

Gradl R, Dierolf M, Yang L, Hehn L, Günther B, Möller W, … & Morgan KS (2019). Visualizing treatment delivery and deposition in mouse lungs using in vivo x-ray imaging. Journal of Controlled Release 307, 282–291. doi:10.1016/j.jconrel.2019.06.035. [PubMed: 31254554]

Greenblatt EE, Winkler T, Harris RS, Kelly VJ, Kone M, and Venegas J (2015). Analysis of Three-Dimensional Aerosol Deposition in Pharmacologically Relevant Terms: Beyond Black or White ROIs. J Aerosol Med Pulm Drug Deliv 28(2):116–129. doi:10.1089/jamp.2013.1120. [PubMed: 25050754]

Hofmann W, Balásházy I, and Heistracher T (2001). The Relationship between Secondary Flows and Particle Deposition Patterns in Airway Bifurcations. Aerosol Science and Technology 35(6):958–968. doi:10.1080/027868201753306723.

Hofmann W (2011). Modelling inhaled particle deposition in the human lung—A review. Journal of Aerosol Science 42(10), 693–724. doi:10.1016/j.jaerosci.2011.05.007.

Hussain M, Madl P, & Khan A (2011). Lung deposition predictions of airborne particles and the emergence of contemporary diseases, Part-I. Health, 2(2):51–59.

Kala S, & Saylor J (2021). Effect of relative humidity on particle bounce in inertial impactors. In APS Division of Fluid Dynamics Meeting Abstracts P27–002.

Kaye SR and Phillips CG (1997). The influence of the branching pattern of the conducting airways on flow and aerosol deposition parameters in the human, dog, rat and hamster. J Aerosol Sci 28(7):1291–1300. doi:10.1016/S0021-8502(97)00024-4.

Lai CY, Huang SH, Chang CP, & Lin JY (2008). Reducing particle bounce and loading effect for a multi-hole impactor. Aerosol science and technology 42(2):114–122. doi: 10.1080/02786820701809045.

Lenz AG, Karg E, Lentner B, Dittrich V, Brandenberger C, Rothen-Rutishauser B, Schulz H, Ferron GA, and Schmid O (2009). A dose-controlled system for air-liquid interface cell exposure and application to zinc oxide nanoparticles. Part Fibre Toxicol 6(1):32. doi:10.1186/1743-8977-6-32. [PubMed: 20015351]

Lenz AG, Stoeger T, Cei D, Schmidmeir M, Semren N, Burgstaller G, … & Schmid O (2014). Efficient bioactive delivery of aerosolized drugs to human pulmonary epithelial cells cultured in air–liquid interface conditions. American journal of respiratory cell and molecular biology 51(4), 526–535. doi:10.1165/rcmb.2013-0479OC. [PubMed: 24773184]

Li R, Zhou R, & Zhang J (2018). Function of PM2. 5 in the pathogenesis of lung cancer and chronic airway inflammatory diseases. Oncology letters 15(5), 7506–7514. doi:10.3892/ol.2018.8355. [PubMed: 29725457]

Monteiller C, Tran L, MacNee W, Faux S, Jones A, Miller B, & Donaldson K (2007). The pro-inflammatory effects of low-toxicity low-solubility particles, nanoparticles and fine particles, on epithelial cells in vitro: the role of surface area. Occupational and environmental medicine 64(9), 609–615. doi:10.1136/oem.2005.024802. [PubMed: 17409182]

Nannu Shankar S, Mital K, Le E, Lewis GS, Eiguren-Fernandez A, Sabo-Attwood T, & Wu CY (2023). Assessment of Scanning Mobility Particle Sizer (SMPS) for online monitoring of

delivered dose in an *in vitro* aerosol exposure system. Toxicology in vitro 92:105650. doi:10.1016/j.tiv.2023.105650. [PubMed: 37463634]

NJHealth. (2016). Hazardous substance fact sheet: Copper. https://nj.gov/health/eoh/rtkweb/documents/fs/0528.pdf (Accessed 26 July 2023).

Oldham MJ, Castro N, Zhang J, Lucci F, Kosachevsky P, Rostami AA, Gilman IG, Pithawalla YB, Kuczaj AK, Hoeng J, and Lee KM (2020a). Comparison of experimentally measured and computational fluid dynamic predicted deposition and deposition uniformity of monodisperse solid particles in the Vitrocell® AMES 48 air-liquid-interface in-vitro exposure system. Toxicology in Vitro 67:104870. doi:10.1016/j.tiv.2020.104870. [PubMed: 32330563]

Oldham MJ, Castro N, Zhang J, Rostami A, Lucci F, Pithawalla Y, Kuczaj AK, Gilman IG, Kosachevsky P, Hoeng J, and Lee KM (2020b). Deposition efficiency and uniformity of monodisperse solid particle deposition in the Vitrocell® 24/48 Air–Liquid-Interface *in vitro* exposure system. Aerosol Science and Technology 54(1):52–65. doi:10.1080/02786826.2019.1676877.

Paur HR, Cassee FR, Teeguarden J, Fissan H, Diabate S, Aufderheide M, … &Schmid O (2011). *In-vitro* cell exposure studies for the assessment of nanoparticle toxicity in the lung—A dialog between aerosol science and biology. Journal of aerosol science 42(10), 668–692. doi: 10.1016/j.jaerosci.2011.06.005.

Porra L, Dégrugilliers L, Broche L, Albu G, Strengell S, Suhonen H, Fodor GH, Peták F, Suortti P, Habre W, Sovijärvi ARA, and Bayat S (2018). Quantitative Imaging of Regional Aerosol Deposition, Lung Ventilation and Morphology by Synchrotron Radiation CT. Sci Rep 8(1):3519. doi:10.1038/s41598-018-20986-x. [PubMed: 29476086]

Schlesinger RB, & Lippmann M (1978). Selective particle deposition and bronchogenic carcinoma. Environmental Research 15(3):424–431. doi:10.1016/0013-9351(78)90123-8. [PubMed: 679903]

Schmid O, & Cassee FR (2017). On the pivotal role of dose for particle toxicology and risk assessment: exposure is a poor surrogate for delivered dose. Particle and fibre toxicology 14, 1–5. doi: 10.1186/s12989-017-0233-1. [PubMed: 28069023]

Smith LC, Moreno S, Robertson L, Robinson S, Gant K, Bryant AJ, & Sabo-Attwood T (2018). Transforming growth factor beta1 targets estrogen receptor signaling in bronchial epithelial cells. Respiratory Research 19:1–17. doi:10.1186/s12931-018-0861-5. [PubMed: 29295703]

Soysal U, Géhin E, Marty F, Algré E, Robine E, and Motzkus C (2021). Exploring deposition pattern characteristics of aerosols and bioaerosols by inertial impaction for the development of real-time silicon MEMS mass detection systems. Aerosol Science and Technology 55(4):414–422. doi:10.1080/02786826.2020.1861211.

Tilly TB, Ward RX, Luthra JK, Robinson SE, Eiguren-Fernandez A, Lewis GS, Salisbury RL, Lednicky JA, Sabo-Attwood TL, Hussain SM, and Wu CY (2019). Condensational particle growth device for reliable cell exposure at the air–liquid interface to nanoparticles. Aerosol Science and Technology 53(12):1415–1428. doi:10.1080/02786826.2019.1659938. [PubMed: 33033421]

Tilly TB, Ward RX, Morea AF, Nelson MT, Robinson SE, Eiguren-Fernandez A, … & Wu CY (2023). Toxicity assessment of CeO_2 and CuO nanoparticles at the air-liquid interface using bioinspired condensational particle growth. Hygiene and environmental health advances 7:100074. doi:10.1016/j.heha.2023.100074. [PubMed: 37711680]

USEPA. (2023). Alternative Test Methods and Strategies to Reduce Vertebrate Animal Testing. https://www.epa.gov/assessing-and-managing-chemicals-under-tsca/alternative-test-methods-and-strategies-reduce (Accessed 26 December 2023).

Ward RX, Tilly TB, Mazhar SI, Robinson SE, Eiguren-Fernandez A, Wang J, Sabo-Attwood T, and Wu CY (2020). Mimicking the human respiratory system: Online in vitro cell exposure for toxicity assessment of welding fume aerosol. J Hazard Mater 395. doi:10.1016/j.jhazmat.2020.122687.

Yang L, Feuchtinger A, Möller W, Ding Y, Kutschke D, Möller G, … & Schmid O (2019). Three-dimensional quantitative co-mapping of pulmonary morphology and nanoparticle distribution with cellular resolution in nondissected murine lungs. ACS nano 13(2), 1029–1041. doi:10.1021/acsnano.8b07524. [PubMed: 30566327]

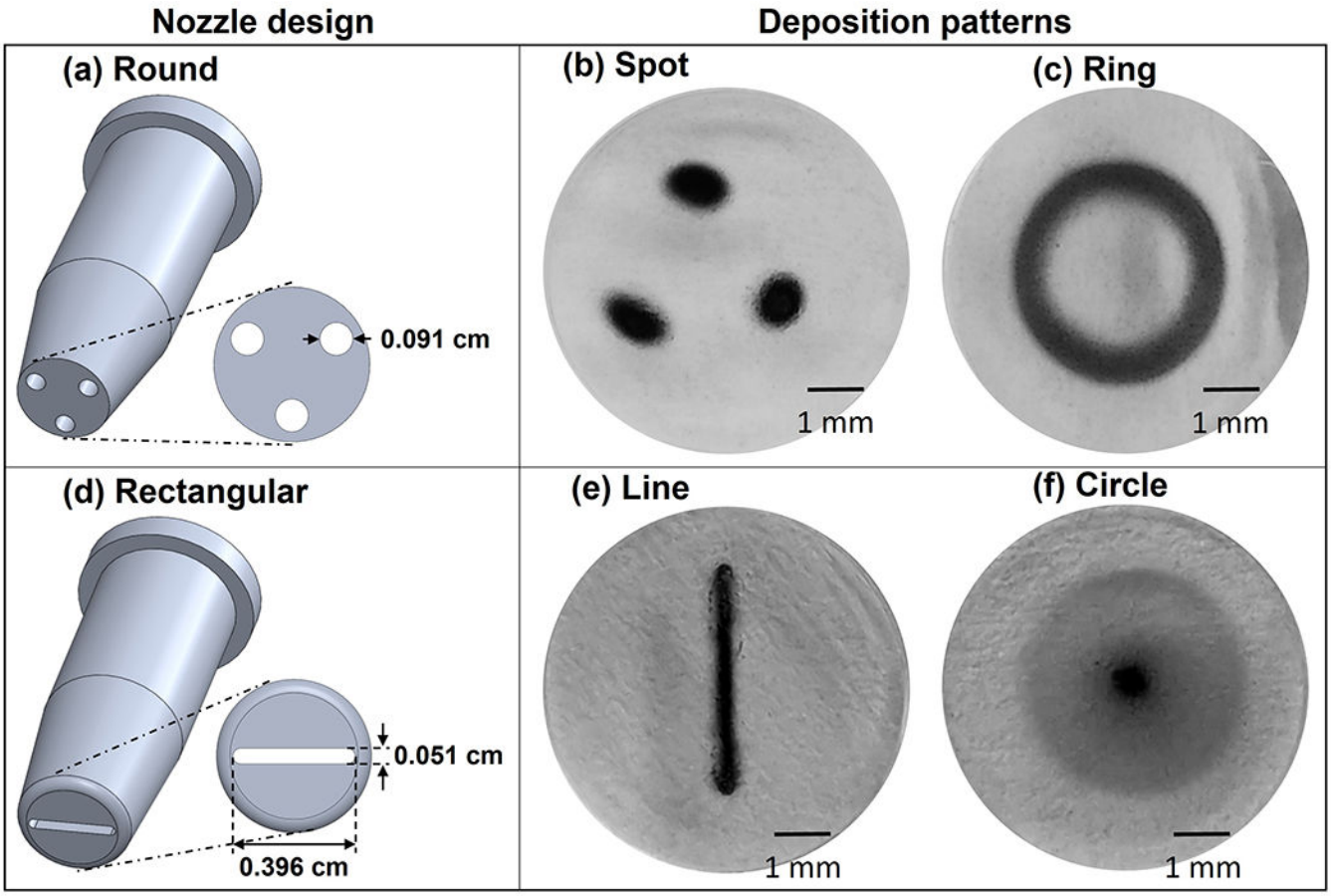

Figure 1.

Round (a) and rectangular (d) nozzles used for deposition in different patterns. Particles are delivered as spot (b) and ring (c) through the round nozzles; while line (e) and circle (f) patterns are obtained through the rectangular nozzles - (c) and (f) are achieved by relative rotation of the collection unit. The patterns in b, c, e and f represent deposition of CuONPs.

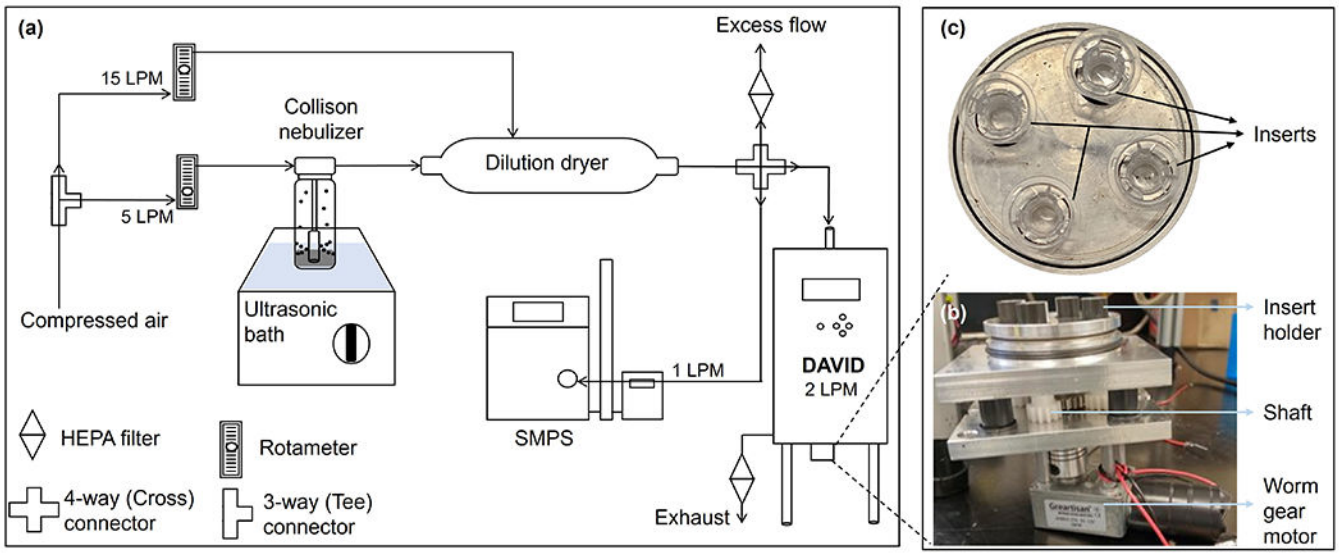

Figure 2.

(a) Experimental setup for delivery of CuONPs to A549 cells at the ALI through DAVID; (b) sample holder (front view) and (c) top view of the sample holder containing the inserts.

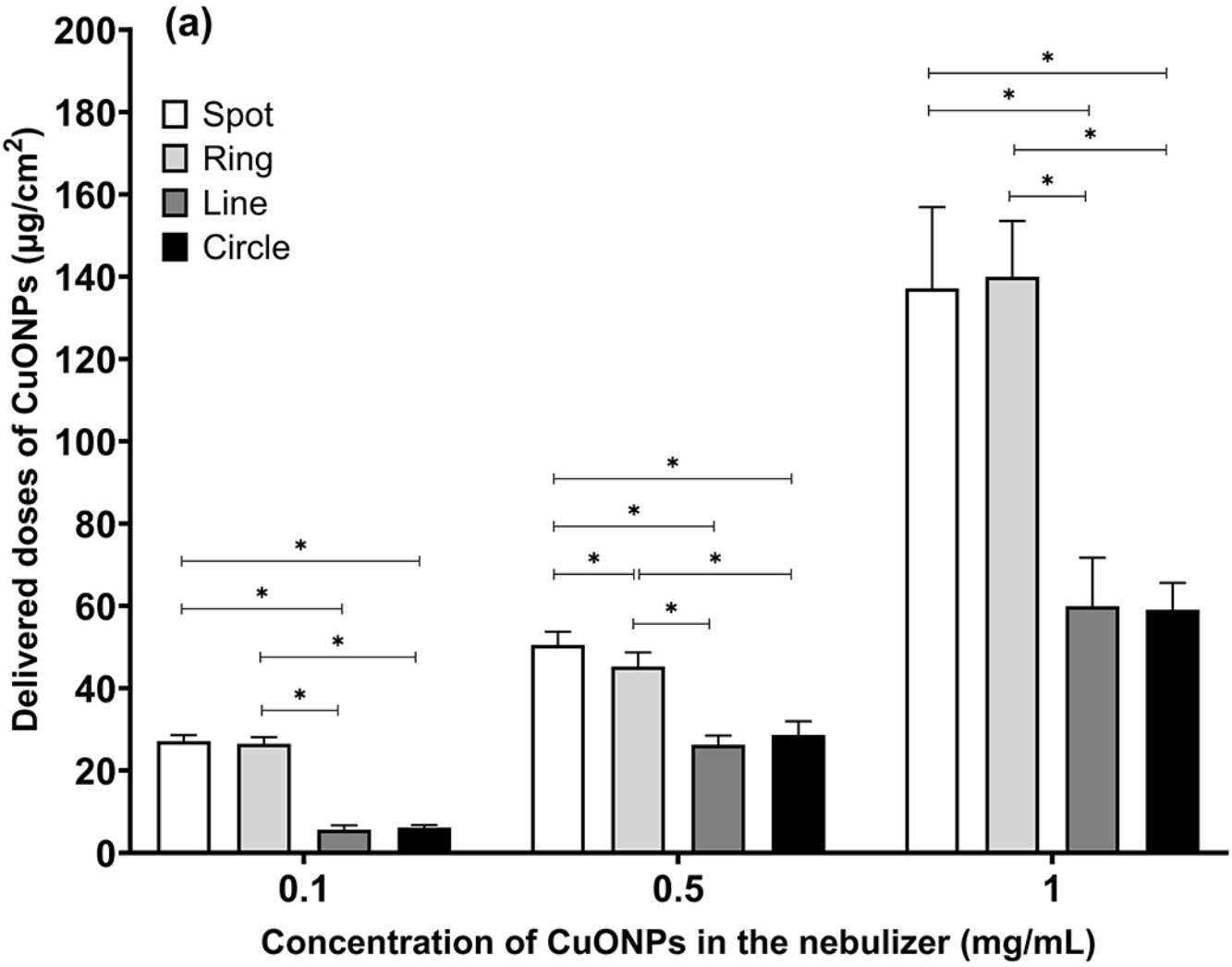

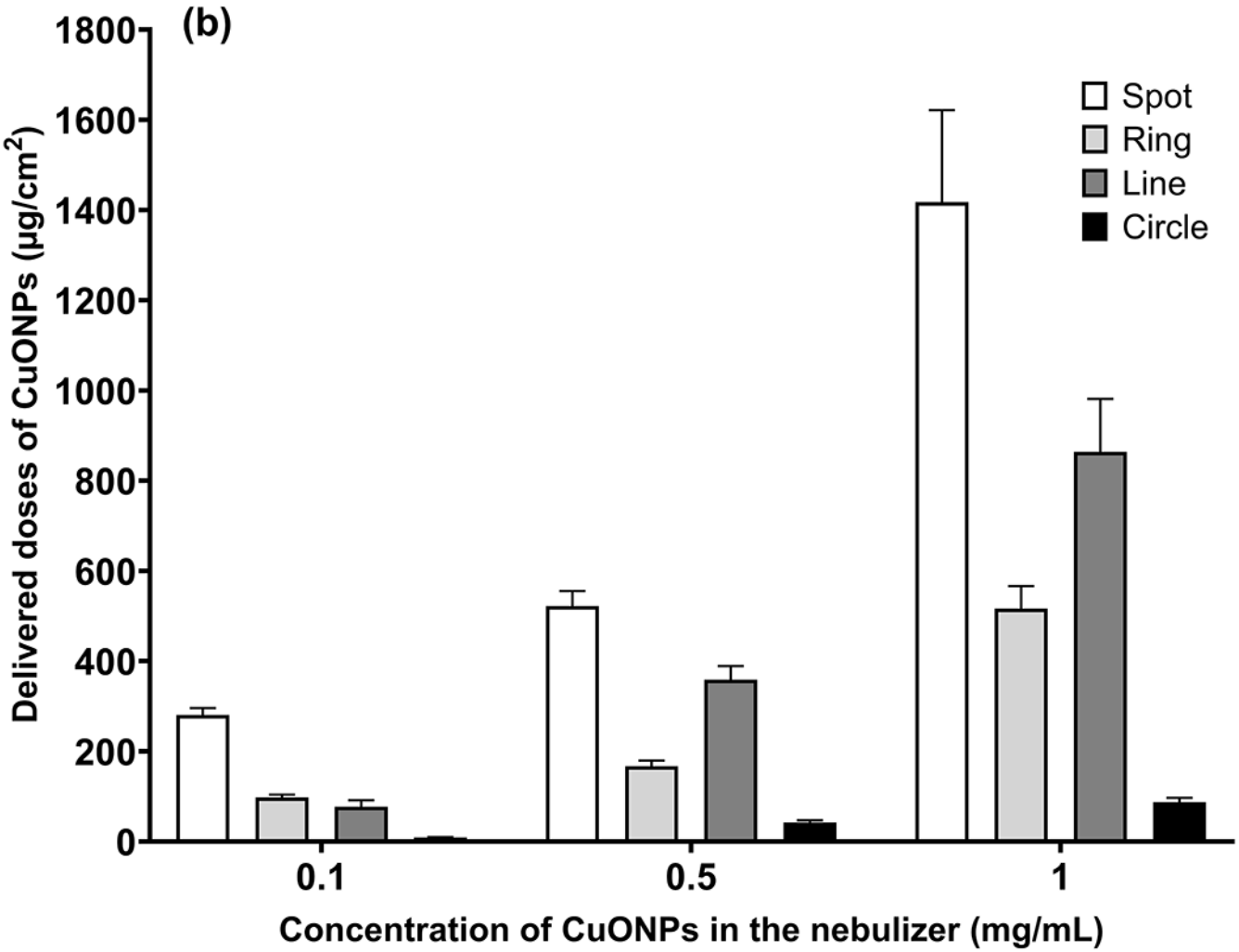

Figure 3.

Performance characteristics of DAVID. (a) Area-averaged doses and (b) Hot spot doses of CuONPs delivered through DAVID in different particle deposition patterns at varying nebulizer concentrations for 15 min of delivery time (✱ in Fig 3a indicates $p \leq 0.05$).

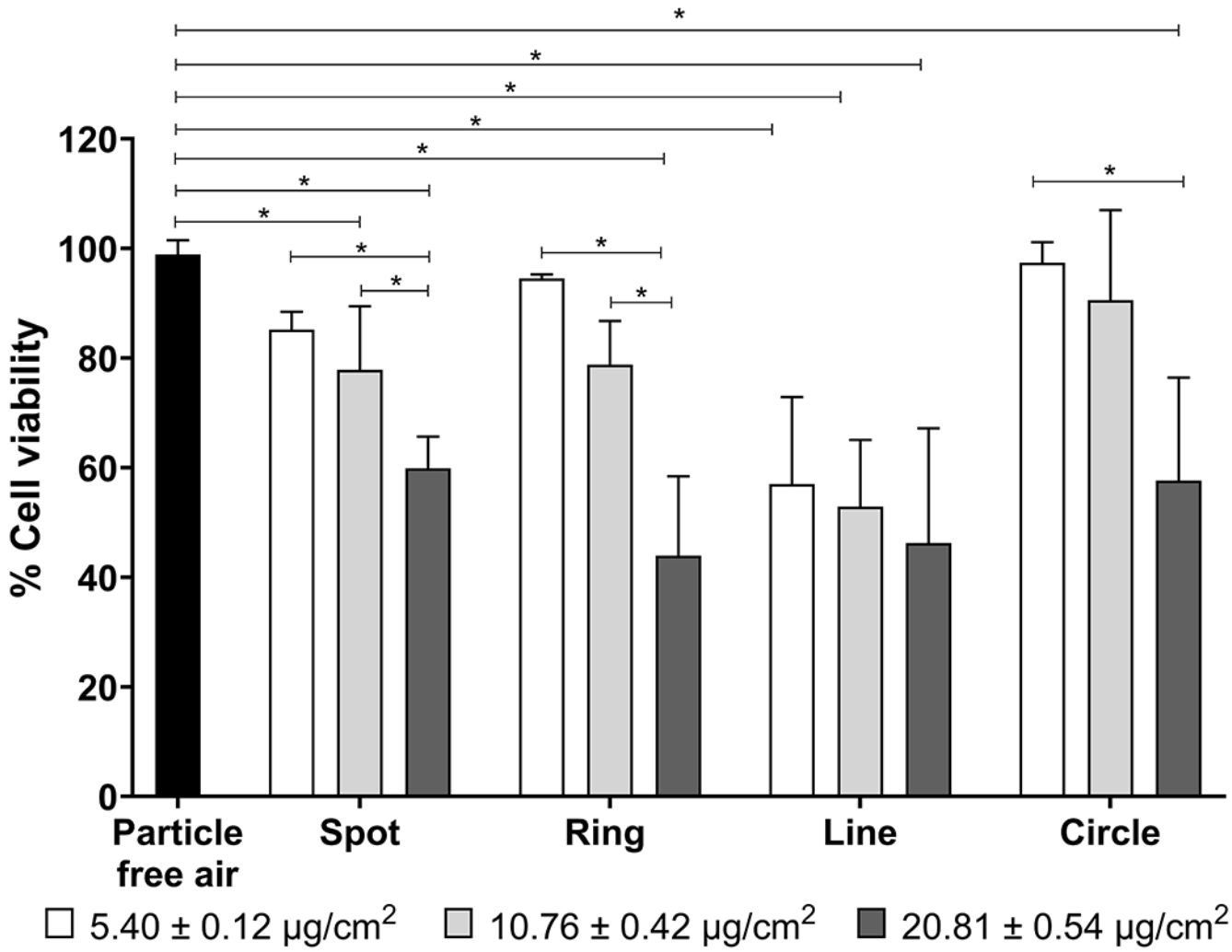

Figure 4.

Cell viability recorded by the alamarBlue assay for varying doses of CuONPs deposited in different deposition patterns to A549 cells cultured at the ALI (✱ indicates p≤0.05).

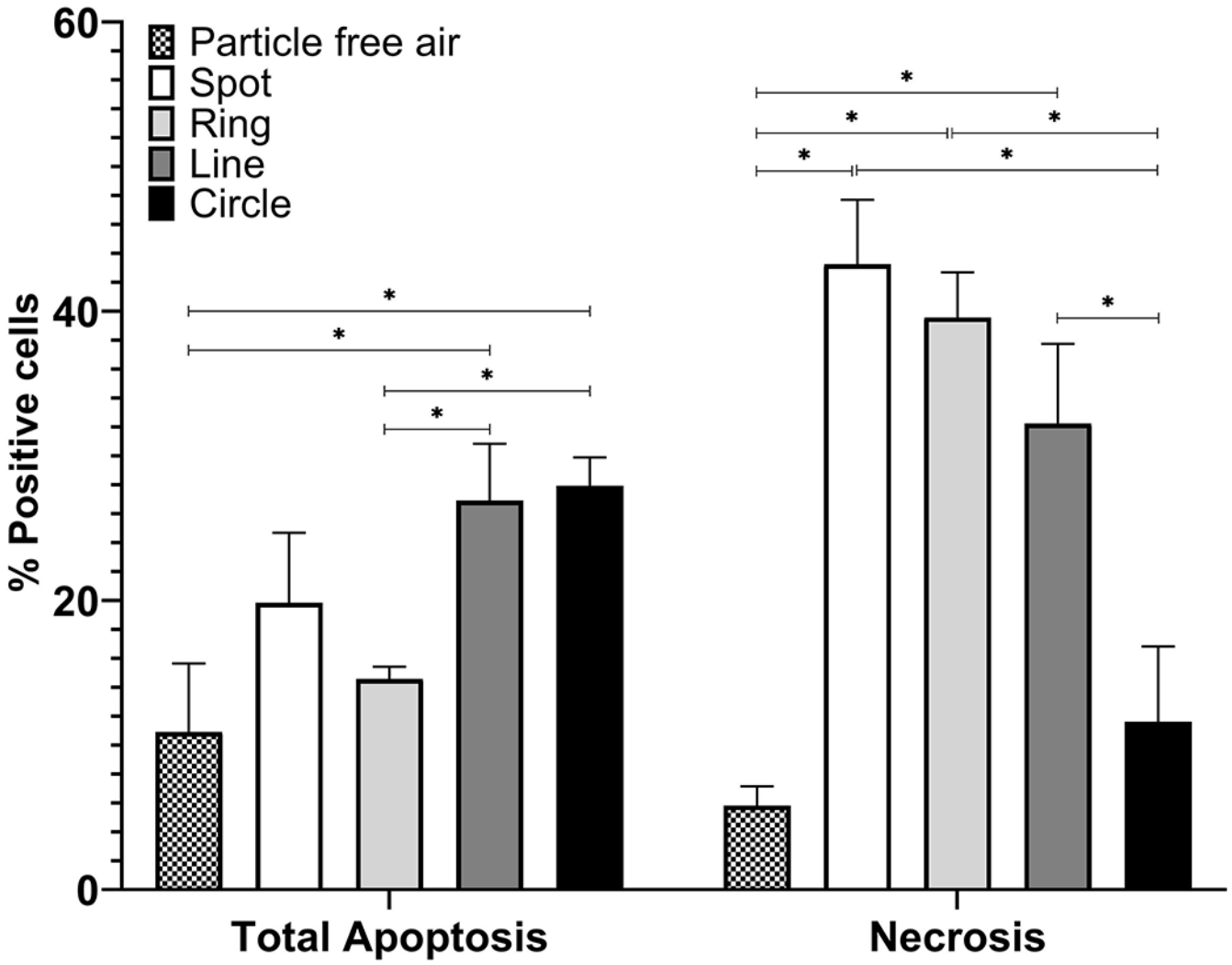

Figure 5.
Cell death by apoptosis and necrosis following a 24 h exposure of A549 cells to ~10 μg/cm^2 of CuONPs, as measured using flow cytometry (✱ indicates p≤0.05).

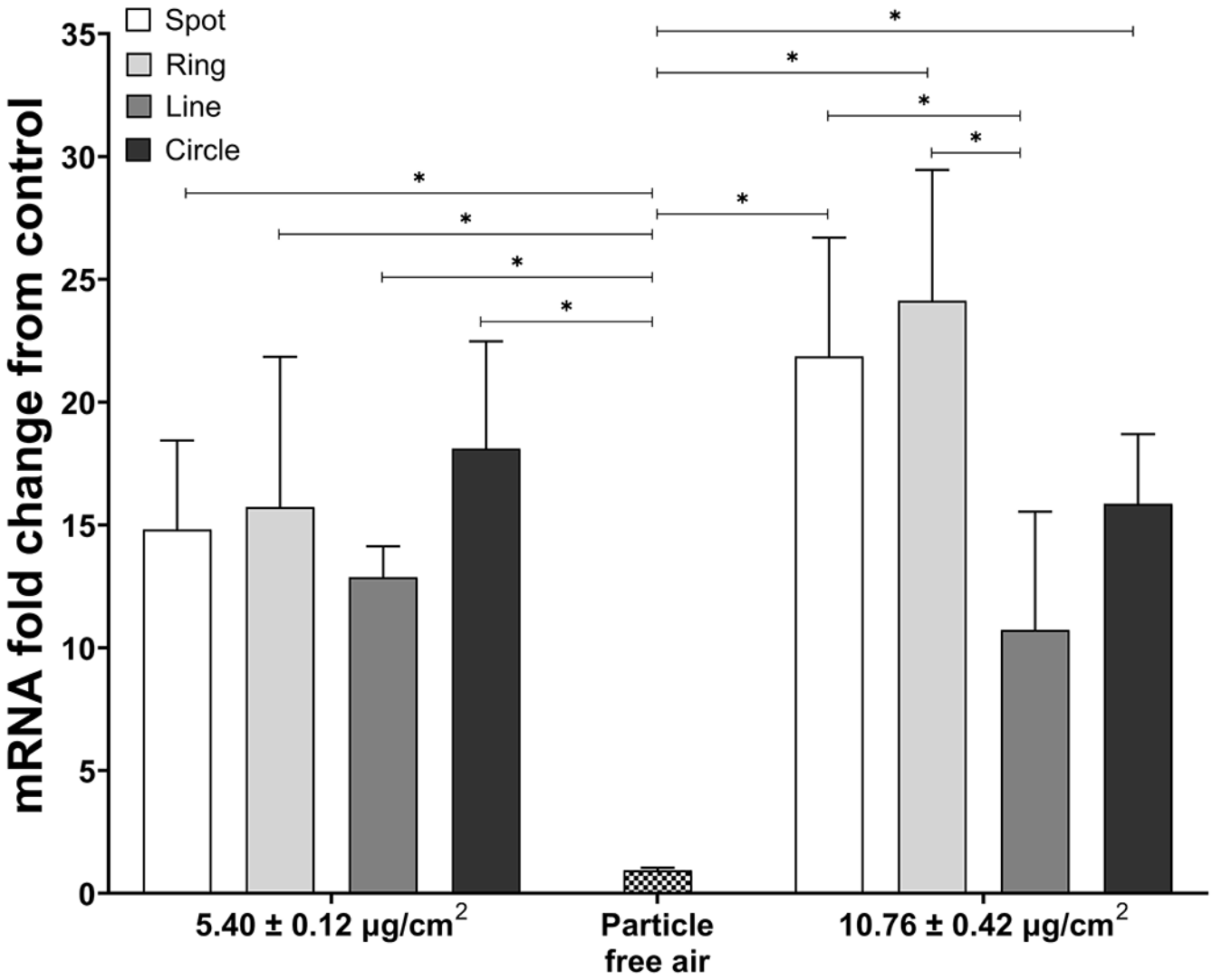

Figure 6.

mRNA expression of HMOX1 following a 24 h exposure of A549 cells to ~5 and 10 µg/cm^2 of CuONPs (✱ indicates p≤0.05).

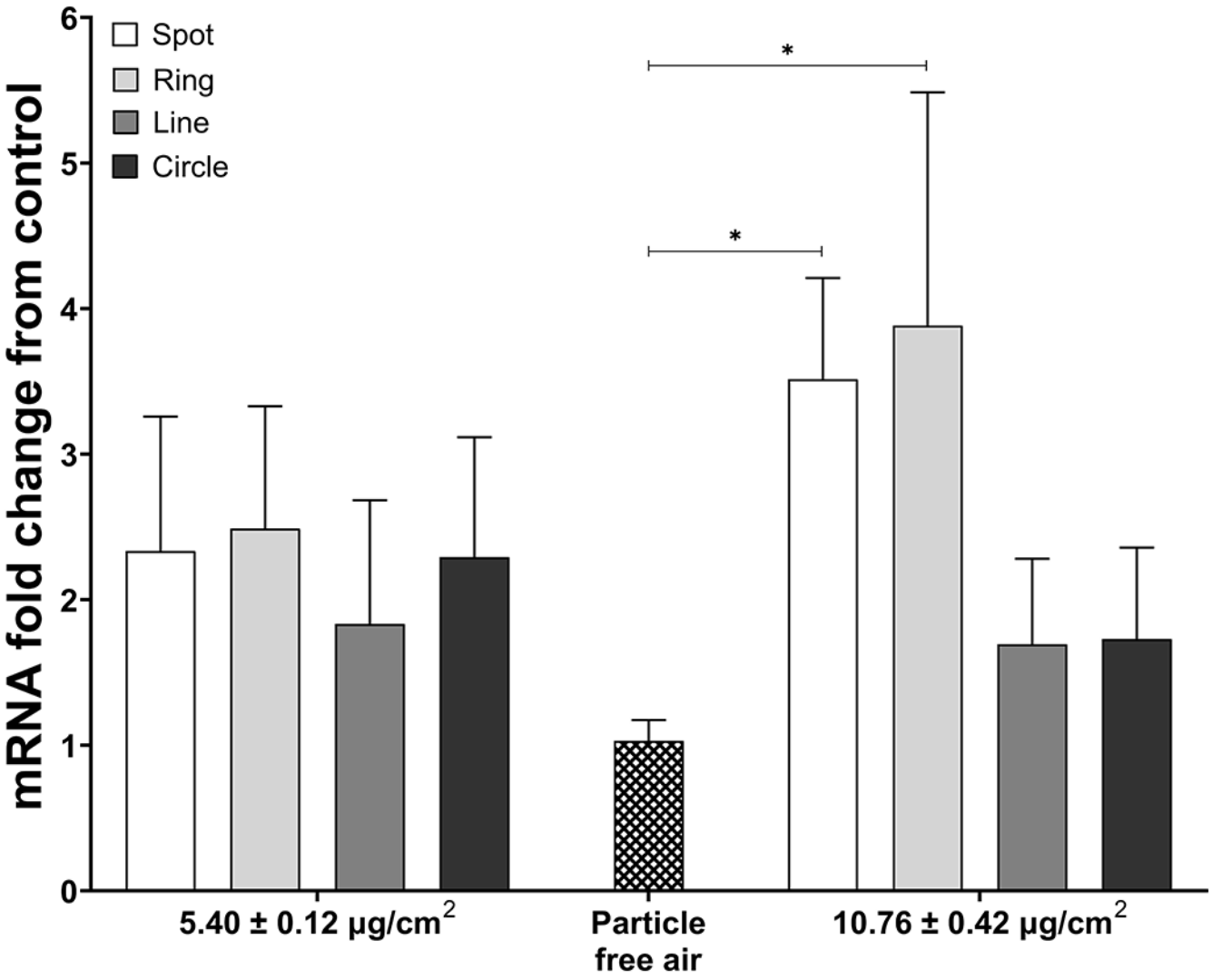

Figure 7.
mRNA expression of IL-8 following a 24 h exposure of A549 cells to ~5 and 10 µg/cm^2 of CuONPs (✱ indicates p≤0.05).